EUROPEAN LABORATORY FOR PARTICLE PHYSICS

CERN-PPE/96-192
17^{th} December 1996

B* production in Z^0 decays

The OPAL Collaboration

Abstract

The process $B^* \to B\gamma$ has been observed in a sample of approximately 4.1 million hadronic Z^0 decays collected by the OPAL detector at LEP in the years 1991–1995. Inclusively reconstructed B mesons have been combined with converted photons to reconstruct approximately 1900 B^* mesons. The B^*–B mass difference is found to be

$$\Delta M(B^* - B) = 46.2 \pm 0.3 \pm 0.8 \text{ MeV}/c^2,$$

and the rate of B^* meson production relative to that of B mesons is found to be

$$\sigma_{B^*}/\sigma_B = 0.760 \pm 0.036 \pm 0.083,$$

where the first errors are statistical and the second systematic. The angular distribution of the transition photon in the B^* rest frame has been measured and the relative contribution of longitudinal B^* polarization states found to be

$$\sigma_l/(\sigma_l + \sigma_t) = 0.36 \pm 0.06 \pm 0.07,$$

consistent with a simple spin counting picture. These results average over B^0, $B^\pm$ and B_s^0 mesons.

(Submitted to Zeitschrift für Physik C)

The OPAL Collaboration

K. Ackerstaff[8], G. Alexander[23], J. Allison[16], N. Altekamp[5], K. Ametewee[25], K.J. Anderson[9], S. Anderson[12], S. Arcelli[2], S. Asai[24], D. Axen[29], G. Azuelos[18,a], A.H. Ball[17], E. Barberio[8], R.J. Barlow[16], R. Bartoldus[3], J.R. Batley[5], J. Bechtluft[14], C. Beeston[16], T. Behnke[8], A.N. Bell[1], K.W. Bell[20], G. Bella[23], S. Bentvelsen[8], P. Berlich[10], S. Bethke[14], O. Biebel[14], A. Biguzzi[2], V. Blobel[27], I.J. Bloodworth[1], J.E. Bloomer[1], M. Bobinski[10], P. Bock[11], H.M. Bosch[11], M. Boutemeur[34], B.T. Bouwens[12], S. Braibant[12], R.M. Brown[20], H.J. Burckhart[8], C. Burgard[8], R. Bürgin[10], P. Capiluppi[2], R.K. Carnegie[6], A.A. Carter[13], J.R. Carter[5], C.Y. Chang[17], D.G. Charlton[1,b], D. Chrisman[4], P.E.L. Clarke[15], I. Cohen[23], J.E. Conboy[15], O.C. Cooke[16], M. Cuffiani[2], S. Dado[22], C. Dallapiccola[17], G.M. Dallavalle[2], S. De Jong[12], L.A. del Pozo[8], K. Desch[3], M.S. Dixit[7], E. do Couto e Silva[12], M. Doucet[18], E. Duchovni[26], G. Duckeck[34], I.P. Duerdoth[16], J.E.G. Edwards[16], P.G. Estabrooks[6], H.G. Evans[9], M. Evans[13], F. Fabbri[2], P. Fath[11], F. Fiedler[27], M. Fierro[2], H.M. Fischer[3], R. Folman[26], D.G. Fong[17], M. Foucher[17], A. Fürtjes[8], P. Gagnon[7], A. Gaidot[21], J.W. Gary[4], J. Gascon[18], S.M. Gascon-Shotkin[17], N.I. Geddes[20], C. Geich-Gimbel[3], F.X. Gentit[21], T. Geralis[20], G. Giacomelli[2], P. Giacomelli[4], R. Giacomelli[2], V. Gibson[5], W.R. Gibson[13], D.M. Gingrich[30,a], D. Glenzinski[9], J. Goldberg[22], M.J. Goodrick[5], W. Gorn[4], C. Grandi[2], E. Gross[26], J. Grunhaus[23], M. Gruwé[8], C. Hajdu[32], G.G. Hanson[12], M. Hansroul[8], M. Hapke[13], C.K. Hargrove[7], P.A. Hart[9], C. Hartmann[3], M. Hauschild[8], C.M. Hawkes[5], R. Hawkings[8], R.J. Hemingway[6], M. Herndon[17], G. Herten[10], R.D. Heuer[8], M.D. Hildreth[8], J.C. Hill[5], S.J. Hillier[1], T. Hilse[10], P.R. Hobson[25], R.J. Homer[1], A.K. Honma[28,a], D. Horváth[32,c], R. Howard[29], R.E. Hughes-Jones[16], D.E. Hutchcroft[5], P. Igo-Kemenes[11], D.C. Imrie[25], M.R. Ingram[16], K. Ishii[24], A. Jawahery[17], P.W. Jeffreys[20], H. Jeremie[18], M. Jimack[1], A. Joly[18], C.R. Jones[5], G. Jones[16], M. Jones[6], R.W.L. Jones[8], U. Jost[11], P. Jovanovic[1], T.R. Junk[8], D. Karlen[6], K. Kawagoe[24], T. Kawamoto[24], R.K. Keeler[28], R.G. Kellogg[17], B.W. Kennedy[20], B.J. King[8], J. Kirk[29], S. Kluth[8], T. Kobayashi[24], M. Kobel[10], D.S. Koetke[6], T.P. Kokott[3], M. Kolrep[10], S. Komamiya[24], T. Kress[11], P. Krieger[6], J. von Krogh[11], P. Kyberd[13], G.D. Lafferty[16], H. Lafoux[21], R. Lahmann[17], W.P. Lai[19], D. Lanske[14], J. Lauber[15], S.R. Lautenschlager[31], J.G. Layter[4], D. Lazic[22], A.M. Lee[31], E. Lefebvre[18], D. Lellouch[26], J. Letts[2], L. Levinson[26], C. Lewis[15], S.L. Lloyd[13], F.K. Loebinger[16], G.D. Long[17], M.J. Losty[7], J. Ludwig[10], A. Malik[21], M. Mannelli[8], S. Marcellini[2], C. Markus[3], A.J. Martin[13], J.P. Martin[18], G. Martinez[17], T. Mashimo[24], W. Matthews[25], P. Mättig[3], W.J. McDonald[30], J. McKenna[29], E.A. Mckigney[15], T.J. McMahon[1], A.I. McNab[13], R.A. McPherson[8], F. Meijers[8], S. Menke[3], F.S. Merritt[9], H. Mes[7], J. Meyer[27], A. Michelini[2], G. Mikenberg[26], D.J. Miller[15], R. Mir[26], W. Mohr[10], A. Montanari[2], T. Mori[24], M. Morii[24], U. Müller[3], K. Nagai[26], I. Nakamura[24], H.A. Neal[8], B. Nellen[3], B. Nijjhar[16], R. Nisius[8], S.W. O'Neale[1], F.G. Oakham[7], F. Odorici[2], H.O. Ogren[12], N.J. Oldershaw[16], T. Omori[24], M.J. Oreglia[9], S. Orito[24], J. Pálinkás[33,d], G. Pásztor[32], J.R. Pater[16], G.N. Patrick[20], J. Patt[10], M.J. Pearce[1], S. Petzold[27], P. Pfeifenschneider[14], J.E. Pilcher[9], J. Pinfold[30], D.E. Plane[8], P. Poffenberger[28], B. Poli[2], A. Posthaus[3], H. Przysiezniak[30], D.L. Rees[1], D. Rigby[1], S. Robertson[28], S.A. Robins[13], N. Rodning[30], J.M. Roney[28], A. Rooke[15], E. Ros[8], A.M. Rossi[2], M. Rosvick[28], P. Routenburg[30], Y. Rozen[22], K. Runge[10], O. Runolfsson[8], U. Ruppel[14], D.R. Rust[12],

R. Rylko[25], K. Sachs[10], E.K.G. Sarkisyan[23], M. Sasaki[24], C. Sbarra[2], A.D. Schaile[34], O. Schaile[34], F. Scharf[3], P. Scharff-Hansen[8], P.. Schenk[34], B. Schmitt[8], S. Schmitt[11], M. Schröder[8], H.C. Schultz-Coulon[10], M. Schulz[8], M. Schumacher[3], P. Schütz[3], W.G. Scott[20], T.G. Shears[16], B.C. Shen[4], C.H. Shepherd-Themistocleous[8], P. Sherwood[15], G.P. Siroli[2], A. Sittler[27], A. Skillman[15], A. Skuja[17], A.M. Smith[8], T.J. Smith[28], G.A. Snow[17], R. Sobie[28], S. Söldner-Rembold[10], R.W. Springer[30], M. Sproston[20], A. Stahl[3], M. Steiert[11], K. Stephens[16], J. Steuerer[27], B. Stockhausen[3], D. Strom[19], F. Strumia[8], P. Szymanski[20], R. Tafirout[18], S.D. Talbot[1], S. Tanaka[24], P. Taras[18], S. Tarem[22], M. Thiergen[10], M.A. Thomson[8], E. von Törne[3], S. Towers[6], I. Trigger[18], T. Tsukamoto[24], E. Tsur[23], A.S. Turcot[9], M.F. Turner-Watson[8], P. Utzat[11], R. Van Kooten[12], G. Vasseur[21], M. Verzocchi[10], P. Vikas[18], M. Vincter[28], E.H. Vokurka[16], F. Wäckerle[10], A. Wagner[27], C.P. Ward[5], D.R. Ward[5], J.J. Ward[15], P.M. Watkins[1], A.T. Watson[1], N.K. Watson[7], P.S. Wells[8], N. Wermes[3], J.S. White[28], B.. Wilkens[10], G.W. Wilson[27], J.A. Wilson[1], G. Wolf[26], S. Wotton[5], T.R. Wyatt[16], S. Yamashita[24], G. Yekutieli[26], V. Zacek[18]

[1]School of Physics and Space Research, University of Birmingham, Birmingham B15 2TT, UK
[2]Dipartimento di Fisica dell' Università di Bologna and INFN, I-40126 Bologna, Italy
[3]Physikalisches Institut, Universität Bonn, D-53115 Bonn, Germany
[4]Department of Physics, University of California, Riverside CA 92521, USA
[5]Cavendish Laboratory, Cambridge CB3 0HE, UK
[6] Ottawa-Carleton Institute for Physics, Department of Physics, Carleton University, Ottawa, Ontario K1S 5B6, Canada
[7]Centre for Research in Particle Physics, Carleton University, Ottawa, Ontario K1S 5B6, Canada
[8]CERN, European Organisation for Particle Physics, CH-1211 Geneva 23, Switzerland
[9]Enrico Fermi Institute and Department of Physics, University of Chicago, Chicago IL 60637, USA
[10]Fakultät für Physik, Albert Ludwigs Universität, D-79104 Freiburg, Germany
[11]Physikalisches Institut, Universität Heidelberg, D-69120 Heidelberg, Germany
[12]Indiana University, Department of Physics, Swain Hall West 117, Bloomington IN 47405, USA
[13]Queen Mary and Westfield College, University of London, London E1 4NS, UK
[14]Technische Hochschule Aachen, III Physikalisches Institut, Sommerfeldstrasse 26-28, D-52056 Aachen, Germany
[15]University College London, London WC1E 6BT, UK
[16]Department of Physics, Schuster Laboratory, The University, Manchester M13 9PL, UK
[17]Department of Physics, University of Maryland, College Park, MD 20742, USA
[18]Laboratoire de Physique Nucléaire, Université de Montréal, Montréal, Quebec H3C 3J7, Canada
[19]University of Oregon, Department of Physics, Eugene OR 97403, USA
[20]Rutherford Appleton Laboratory, Chilton, Didcot, Oxfordshire OX11 0QX, UK
[21]CEA, DAPNIA/SPP, CE-Saclay, F-91191 Gif-sur-Yvette, France

[22]Department of Physics, Technion-Israel Institute of Technology, Haifa 32000, Israel
[23]Department of Physics and Astronomy, Tel Aviv University, Tel Aviv 69978, Israel
[24]International Centre for Elementary Particle Physics and Department of Physics, University of Tokyo, Tokyo 113, and Kobe University, Kobe 657, Japan
[25]Brunel University, Uxbridge, Middlesex UB8 3PH, UK
[26]Particle Physics Department, Weizmann Institute of Science, Rehovot 76100, Israel
[27]Universität Hamburg/DESY, II Institut für Experimental Physik, Notkestrasse 85, D-22607 Hamburg, Germany
[28]University of Victoria, Department of Physics, P O Box 3055, Victoria BC V8W 3P6, Canada
[29]University of British Columbia, Department of Physics, Vancouver BC V6T 1Z1, Canada
[30]University of Alberta, Department of Physics, Edmonton AB T6G 2J1, Canada
[31]Duke University, Dept of Physics, Durham, NC 27708-0305, USA
[32]Research Institute for Particle and Nuclear Physics, H-1525 Budapest, P O Box 49, Hungary
[33]Institute of Nuclear Research, H-4001 Debrecen, P O Box 51, Hungary
[34]Ludwigs-Maximilians-Universität München, Sektion Physik, Am Coulombwall 1, D-85748 Garching, Germany

[a] and at TRIUMF, Vancouver, Canada V6T 2A3
[b] and Royal Society University Research Fellow
[c] and Institute of Nuclear Research, Debrecen, Hungary
[d] and Department of Experimental Physics, Lajos Kossuth University, Debrecen, Hungary

1 Introduction

The B^* is the well established vector partner of the pseudoscalar B meson, the mass difference between the B^* and B being $\sim$ 46 MeV/c^2 [1]. Due to the small B^*–B mass difference, all strong decays of the B^* are forbidden, implying a branching ratio for the electromagnetic decay $B^* \to B\gamma$ close to 100% . In a simple spin counting model the relative rate of primary vector particle production to the sum of vector plus pseudoscalar production, V/(V+P), would be 0.75. However in an analysis such as this an *effective* V/(V+P) is measured that can be defined as the relative measured rate of B^* to B meson production σ_{B^*}/σ_B, where this is the inclusive ratio of the number of observed B^* mesons to the number of observed B mesons. This measured rate differs from primary production expectations due to the contribution of higher resonances, where the relative decay rates to the ground state and excited states are unknown, and from phase-space effects arising from the mass difference between the vector and pseudoscalar states. The same arguments are true of K^* and D^* production, where values much lower than 0.75 are found. Indeed in the D sector even after accounting for higher resonances and phase-space effects, the primary vector to vector plus pseudoscalar rates are measured to be far from 3/4, as discussed in Reference [2]. Phase-space effects are expected to be negligible for B mesons (since the $B^* - B$ mass splitting is small) and thus the principal uncertainties in the expected production rate arise from the fact that for some higher resonances decays to either the spin 1 or spin 0 ground states are forbidden by spin and parity conservation.

In the measurement described here B mesons have been reconstructed inclusively and combined with converted photons whose energy and momentum is reconstructed from the e^+ and e^- tracks. Measurements are presented of the B^*–B mass difference and the production rate of the B^* meson relative to that of the B meson, σ_{B^*}/σ_B. Additionally, the relative contribution of the longitudinally polarized B^* state has been measured, using the angular distribution of the photons in the B^* rest frame.

2 The OPAL detector

The OPAL detector has been described elsewhere [3] and will be discussed only briefly here. The central detector consists of three wire chambers: a large volume jet chamber which measures particle trajectories and ionisation energy loss (dE/dx), a smaller vertex drift chamber, and a set of planar drift chambers surrounding the jet chamber, oriented to measure the z coordinate.[1] These detectors are operated in a pressure vessel at 4 bar. Between the pressure vessel and a beryllium beam pipe are two layers of silicon strip detectors [4]. In this analysis only information from the strips oriented parallel to the beam axis was used. The entire central detector is inside a uniform axial magnetic field of 0.435 T. The region outside the coil is instrumented with time-of-flight counters, and in both the barrel and the endcap regions lead-glass electromagnetic calorimeters are preceded by presamplers. The iron return yoke of the magnet is instrumented as a hadron calorimeter, and four layers of muon chambers are located outside the iron.

[1] The OPAL coordinate system is defined with positive z along the electron beam direction and θ and ϕ as the polar and azimuthal angles, respectively. The radial coordinate is denoted by r.

3 Event selection and Monte Carlo description

3.1 Event selection

Hadronic Z^0 decays are selected using the criteria described in Reference [5]. Charged tracks and electromagnetic clusters not associated with any charged track are grouped into jets using a cone jet algorithm [6]. The primary event vertex is reconstructed using the charged tracks in the event along with knowledge of the average position and effective spread of the e^+e^- collision point.

The analysis is performed on data collected in the vicinity of the Z^0 peak from 1991 through 1995. A total of about 4.1 million hadronic events satisfied the event selection criteria.

3.2 Description of the Monte Carlo

Monte Carlo events are used to compare with experimental distributions and to calculate the efficiencies of the selection criteria. The JETSET 7.4 Monte Carlo program [7, 8] was used to generate $Z^0 \rightarrow q\bar{q}$ decays which were processed by the detector simulation program [9].

The fragmentation parametrisation is that of Peterson *et al.* [10], with $\epsilon_b = 0.0057$ and $\epsilon_c = 0.046$, for b and c quarks, respectively, corresponding to mean scaled energies, $\langle x_E \rangle$, of 0.700 and 0.508. The samples contain B^* mesons generated with mass differences with respect to the corresponding B meson of 46.0, 46.3 and 46.7 MeV/c^2 for the u, d and s species, respectively. These values were motivated by measurements of the average mass difference at LEP and elsewhere [1]. All Monte Carlo samples included production of p-wave mesons, with primary production fractions for the b sector of 37% for the u and d states and 39% for the s states. The masses of the four p-wave states were chosen for consistency with both recent measurements of these states at LEP [1, 11, 12], and with the model of Eichten, Hill and Quigg [13], where heavy quark symmetry is used to estimate both masses and widths of such states.

4 Inclusive b hadron reconstruction

The inclusive reconstruction of b hadrons starts with a jet in which a secondary vertex has been found. The following sections describe the secondary vertex selection and the estimators for the b hadron direction and energy. Both the vertex reconstruction and the B energy and momentum estimate use the techniques described in Reference [11].

4.1 Vertex selection

The two highest energy jets in each event are searched for secondary vertices in the $r-\phi$ plane. Secondary vertex candidates are accepted if they contain at least three tracks, are separated from the primary vertex by at least five times the uncertainty in the decay length as calculated

using the vertex covariances, and if the output value of an artificial neural network designed to reject non-b background is acceptable.[2] For each secondary vertex candidate the position of the primary vertex is redetermined excluding tracks that were assigned to the secondary vertex.

The positions of the primary and secondary vertices are used to estimate the ϕ angle of the b hadron momentum vector at production. The calculated uncertainty in this angle, based on the vertex positions and covariances, is required to satisfy $\sigma_\phi < 0.035$ radians.

4.2 B momentum vector estimation

For each track in a jet containing an accepted secondary vertex a weight is calculated to assess the probability that the track came from the secondary vertex. The weight is given by

$$\omega' = \frac{R(b/\eta)}{R(b/\eta) + R(d/\sigma)},$$

where R is a symmetric function describing the impact parameter significance of the track in the $r-\phi$ plane with respect to a fitted vertex. The quantities b and η are the impact parameter and its error with respect to the secondary vertex and d and σ are the corresponding quantities with respect to the primary vertex. A correction is applied to this weight as a function of track momentum to account for the fact that more tracks come from the secondary than the primary vertex. This corrected weight, ω, lies in the range [0,1].

The b hadron momentum reconstruction is performed using these corrected weights. An estimate of the charge of each vertex can be calculated and whilst the charge information provided in this way is not useful for B^* reconstruction it can be used to improve the momentum resolution of the b hadron sample since a good charge measurement is highly correlated to the correct assignment of all tracks in a jet to the appropriate vertex. The accuracy of the vertex charge estimate for each vertex can be gauged by its r.m.s.,

$$\sigma_q = \left(\sum_{i=1}^{N_{jet}} \omega_i (1 - \omega_i) \right)^{1/2},$$

where the summation is over the number, N_{jet}, of tracks in the jet.

A cut is made on the quality of the charge reconstruction by demanding that $\sigma_q < 1.0$. This cut removes 35% of those vertices passing all other cuts.

The momentum vector of charged particles coming from the b hadron decay is defined as

$$\mathbf{p}_{vtx} = \sum_{i=1}^{N_{jet}} \omega_i \mathbf{p}_i,$$

where $\mathbf{p}_i$ is the momentum of track i. $\mathbf{p}_{vtx}$ serves as an initial estimate of the B direction. The energies of electromagnetic clusters unassociated with charged tracks and lying within

[2] The neural network has seven input parameters, the most important of which are the decay length, its uncertainty and the vertex multiplicity.

0.4 radians of $\mathbf{p}_{vtx}$ are scaled by 0.7 and their momentum vectors summed to form the vector $\mathbf{p}_{EM}$. The scaling was found to be appropriate to account for neutral energy not associated with the B decay. The direction of the B is calculated using the ϕ angle defined by the flight vector from the primary to the secondary vertex, and using the polar angle of the vector $\mathbf{p}_{vtx}$ + $\mathbf{p}_{EM}$. The distribution of the difference between the reconstructed and generated ϕ angles of the B meson in the simulation can be described by a fit to the sum of two Gaussians. The standard deviation, σ, of the narrower Gaussian is 8 mrad, and 77% of the entries lie within 3σ. The corresponding quantities describing the θ resolution are σ= 15 mrad and 91%, respectively.

The resolution on the measurement of the total energy of the B meson can be improved through the use of a constraint to the LEP beam energy. The knowledge of the total centre-of-mass energy, $E_{CM} = 2E_{\rm beam}$, can be used in conjunction with a measurement of the recoil mass of the rest of the event, m_{rec}, calculated by adding the momenta of all charged tracks and unassociated electromagnetic clusters *not* in the jet of the B candidate. For this calculation m_{jet} is set to the B mass, 5.279 GeV/c^2. Thus the jet energy is calculated from

$$E_{jet}^{tot} = \frac{E_{CM}^2 - m_{rec}^2 + m_{jet}^2}{2E_{CM}}.$$

The B meson energy is then estimated from this total jet energy minus the energy within the jet attributed to fragmentation

$$E_{\rm B} = E_{jet}^{tot} - (E_{jet}^{vis} - E_{vtx} - E_{EM}),$$

where the visible jet energy E_{jet}^{vis} is the sum over all charged tracks and unassociated electromagnetic clusters in the jet and E_{vtx} is the energy defined analogous to $\mathbf{p}_{vtx}$, summing over E_i, and E_{EM} is defined analogous to $\mathbf{p}_{EM}$. For this calculation the pion mass is assumed for all charged particles. Only vertices with $E_{\rm B}$ >15 GeV and $E_{\rm B}/E_{EM}$ >0.65 are used in the analysis. The narrower Gaussian from a two Gaussian fit to the difference between the reconstructed and generated b hadron energy has a width of 2.9 GeV, and 92% of the entries are contained within 3σ. The B meson momentum is given by $\sqrt{E_{\rm B}^2 - m_{\rm B}^2}$, with $m_{\rm B}$ fixed to 5.279 GeV/c^2.

This procedure applied to the Z^0 data taken in 1991–1995 yields approximately 222000 tagged jets with a b purity of 91.7%, as determined from the Monte Carlo. The reconstructed b hadron momentum distribution is shown in Figure 1 for data and Monte Carlo, where the Monte Carlo distribution has been normalised to the total number of hadronic events analysed in the data.

5 Photon reconstruction

The photon produced in the decay $B^* \to B\gamma$ has an energy of $\sim$ 46 MeV in the rest frame of the B^*, limiting its energy in the laboratory to a maximum of about 800 MeV. The mean energy in the laboratory frame of these photons is approximately 350 MeV. Photons that convert

into an e^+e^- pair in the material of the detector are reconstructed by combining the charged tracks of the e^+e^- pair. The conversion probability for photons coming from the decay of the B^* is approximately 8% for photons that convert within the tracking volume, and the resolution for these photons is better than that for unconverted photons reconstructed with the calorimetry. The conversion algorithm selects tracks that have a transverse momentum relative to the beam direction, p_t, greater than 50 MeV and a tangent which points back to the primary vertex in the r-ϕ plane. The point where this tangent meets the track is considered as a potential conversion point. Combinations of all possible pairs of such tracks in an event are made and cuts are applied according to their angular separation at their point of tangency, requiring

- $\Delta\phi$ <40 mrads
- $\Delta\theta$ <50 mrads.

For all pairs of tracks passing these cuts a pseudo χ^2 is constructed from properties of the two individual tracks. This utilises θ, ϕ and R, the distance (in the r-ϕ plane) from the origin to the point on a given track where the tangent to the track passing through the primary vertex meets it. The pseudo χ^2 has the form

$$\chi^2 = \left(\frac{\Delta\theta}{\sigma_\theta}\right)^2 + \left(\frac{\Delta\phi}{\sigma_\phi}\right)^2 + \left(\frac{\Delta R}{\sigma_R}\right)^2 .$$

The resolutions σ_θ and σ_ϕ have been determined from Monte Carlo and σ_R is the sum in quadrature of the errors on R for each of the two tracks.

Pairs of selected tracks passing these cuts are combined, the conversion point fitted in the r-ϕ plane and the momentum components of the two tracks summed at this point to give the photon energy, E_γ. The z position of this vertex is fitted independently and the reconstructed photon vector is constrained to the z coordinate of the primary vertex to improve the accuracy of the θ determination. The flight direction of the photon is calculated relative to the primary vertex and the candidate rejected if this points towards the primary vertex, rather than away from it.

The following cuts are made on the conversion candidate

- Distance of conversion point from primary vertex > 2 cm
- Invariant mass of the e^+e^- pair < 0.1 GeV/c^2.

The conversion candidates are ordered by pseudo χ^2 and pairs selected in order of lowest χ^2, with no track used more than once. No absolute cut on χ^2 is applied. An average of 0.8 conversions are selected per hadronic event.

Figure 2 shows the efficiency and purity of the conversion algorithm as a function of energy, E_γ, for photons with E_γ < 1 GeV, as estimated by Monte Carlo. In this figure efficiency is defined as the fraction of all photons that convert within the OPAL tracking detectors (*i.e.* at

a radius less than 180 cm) that are successfully reconstructed. The purity is the fraction of the conversion sample where the reconstructed e^+ and e^- tracks each arise from separate tracks of the same converted photon.

The total efficiency of the algorithm for reconstructing photons from the decay $B^* \to B\gamma$ is estimated by the Monte Carlo simulation to be (1.41 ± 0.01) %, where this error is statistical.

Fits to the difference between the reconstructed and generated photon energy in Monte Carlo have been made using the sum of two Gaussians of the same mean. The narrower Gaussian has a width of 13 MeV, and 78% of the entries are contained within 3σ. Similar fits to the ϕ and θ resolutions give values of 3 mrad (76%) and 8 mrad (69%), respectively.

6 Reconstruction of $B^* \to B\gamma$ decays

Reconstructed B mesons and photon conversions are combined if they lie in the same hemisphere as defined by the event thrust axis. Three kinematic variables are involved in the determination of the mass difference between the vector and pseudoscalar B mesons: the B momentum, the photon energy and the angle between the B meson and the photon. The mass difference is given to a good approximation by

$$\Delta M(B^* - B) = M(B^*) - M(B) \simeq E_\gamma \gamma_B (1 - \beta_B \cos\alpha),$$

where E_γ is the energy of the photon, γ_B and β_B are the Lorentz factors of the B meson, and α is the opening angle between the reconstructed B and photon directions. The resolution on the mass difference is dominated by the measurement of the opening angle between the photon and the B, and this in turn is dominated by the resolution on the B direction.

6.1 The ΔM measurement

The mass difference ΔM between the B^* and B mesons is calculated by combining the reconstructed B meson with the conversion photon and subtracting the nominal B mass of 5.279 GeV/c^2. The shape of the background is taken from the Monte Carlo simulation. The ΔM distribution observed in the data is shown in Figure 3, with a fit to the Monte Carlo estimation of the background. The dominant contribution to the background, as determined by Monte Carlo simulations, is the random combination of B mesons with converted photons from π^0 decays. The Monte Carlo background has been fitted and normalised to the number of data entries in the sideband region 0.1 GeV/c^2 $< \Delta M <$ 0.2 GeV/c^2. A technique to model the shape of this background using light quark events, to confirm the accuracy of the Monte Carlo simulation, has been developed and is discussed in Section 7.2.

A fit is made to the data plus background, using the functional form for the background obtained from the Monte Carlo[3]. The signal is fitted with the sum of a Gaussian and an

[3]The functional form used is $(P_1 + P_2 x + P_3 x^2) \times (1 - e^{(P_4 x + P_5 x^2)})$, where P_i are the five fitted parameters.

asymmetric Gaussian[4], where both are constrained to have the same peak position. The simple Gaussian has a width of 5.5 ± 0.5 MeV/c^2, and the asymmetric Gaussian widths of 14.6 $\pm$ 1.7 and 18.0 $\pm$ 5.0 MeV/c^2, the two distributions being approximately equally populated. The fit to the data signal and the background subtracted plot are shown in Figure 3.

The result of the fit to the mass difference is

$$\Delta M(\mathrm{B}^* - \mathrm{B}) = 46.2 \pm 0.3(stat.)\ \mathrm{MeV}/c^2,$$

where this measurement averages over all flavours of B mesons.

6.2 Measurement of the B*/B production rate

The relative production rate is defined as the number of B^* mesons produced as a fraction of the total number of B mesons, and can be calculated from the number of observed B^* mesons N_{B^*} via

$$\sigma_{\mathrm{B}^*}/\sigma_{\mathrm{B}} = N_{\mathrm{B}^*}/(N_{jets}\eta_{\mathrm{b}}\epsilon_\gamma f_{\mathrm{B}}).$$

Here N_{jets} is the number of jets selected by the jet and vertex cuts, η_{b} is the purity of the b-jet sample, ϵ_γ is the total efficiency for reconstructing photons from the process $\mathrm{B}^* \rightarrow \mathrm{B}\gamma$, and f_{B} is the fraction of all b quarks that fragment to mesons.

The number of B^* mesons observed in the 222000 jets selected is taken from the result of the fit to the data in Section 6.1. In the combined 1991 to 1995 OPAL data 1894 ± 89 B^* candidates are reconstructed. The photon reconstruction efficiency is measured in Monte Carlo to be $(1.41 \pm 0.01)\%$, and the b purity to be $(91.7 \pm 0.1)\%$, where these errors are statistical.

The value of f_{B} used here has been obtained through a combination of results from LEP experiments [14, 15] and is $(86.8 \pm 4.1)\%$.

The relative production rate is measured to be

$$\sigma_{\mathrm{B}^*}/\sigma_{\mathrm{B}} = 0.760 \pm 0.036(stat.).$$

7 Systematic errors

7.1 Signal shape

The Monte Carlo has been used to determine an appropriate shape for fits to the signal and to confirm that the reconstruction procedure introduces no biases in the ΔM measurement.

[4]The asymmetric Gaussian is a Gaussian bifurcated at the peak position. It thus has the form

$$f(x) = \frac{2}{(\sigma_1+\sigma_2)\sqrt{2\pi}} \begin{cases} e^{-(x-x_0)^2/2{\sigma_1}^2} & \text{for } x < x_0, \\ e^{-(x-x_0)^2/2{\sigma_2}^2} & \text{for } x \geq x_0 \end{cases}$$

The Monte Carlo B^* signal has been fitted with the sum of a Gaussian and an asymmetric Gaussian (see Section 6.1) constrained to the same peak position, as is done for the data. The fit to the Monte Carlo signal is shown in Figure 4. However the shape of the signal in Monte Carlo is somewhat different from that in the data. In the Monte Carlo the tail towards lower values of the mass difference is seen to be significantly smaller than that in the data. Other resolutions seen in the data are well described by the Monte Carlo. Threshold effects are believed to introduce the asymmetry in the signal, and the discrepancy between Monte Carlo and data is thought to be due to inadequacies in the modelling of the effects of radiation from the e^+e^- tracks of the converted photon. This mismodelling can also be seen in the invariant mass distribution of converted photon pairs in the region below the π^0 mass (see Section 7.3 below).

The uncertainty arising from ambiguity over the precise signal shape has been quantified by repeating the fit to the data with the shape constrained to that seen in the Monte Carlo. This exercise results in a change in the fitted B^*–B mass difference of 0.1 MeV/c^2, and an uncertainty in the number of B^* candidates of $\pm$ 30, equivalent to an error of $\pm$ 1.6%. The fit constrained to the shape seen in the Monte Carlo has a χ^2 of 1.5, 25% higher than that in the standard free fit, described in Section 6.1.

7.2 The fit procedure

The shape of the background and the accuracy with which this is duplicated by the Monte Carlo have been studied using a light quark sample to simulate the combinatorial background under the B^* peak. Identical cuts to those applied to the B^* sample are used but with the cut on the secondary vertex separation removed and the b-tagging neural network demand reversed so that events not passing the cut are accepted. In this way an *anti-b* selection is made. Vertices and photons are then reconstructed in an identical way to the B^* analysis. This yields a sample of events with similar properties to the B^* sample but of very low b purity. The distribution of the measured mass difference in these events is shown in Figure 5, where it has been compared with a Monte Carlo sample produced using the same technique and with the Monte Carlo sample used to model the background in the fit to the B^* signal. All distributions agree reasonably well. Figure 5a is used to quantify Monte Carlo-data agreement, using the light quark sample, and Figure 5b to demonstrate that the light quark sample is a useful sample for studying systematic effects due to the Monte Carlo background used in the analysis.

The errors arising from remaining uncertainties in the background shape are quantified by scaling the Monte Carlo background by the ratio of the data to the normalised Monte Carlo distribution from the light quark fake background sample. Thus the fake background is used only as a way of quantifying the uncertainty in the agreement between data and Monte Carlo and does not directly enter into the fit to the signal. The fit to the B^* signal is then repeated using this bin-by-bin scaled background. The results of this fit differ by 0.3 MeV/c^2 in the mass difference and 5.0% in the production rate. These differences are assigned as systematic errors.

The statistical error on the normalisation in the sideband region is 0.4%, which contributes

0.8% to the uncertainty on the number of B^* mesons. There is an additional error on the B^* production rate of 2% arising from uncertainties in the parametrisation of the Monte Carlo background shape. Both effects are a negligible contribution to the error on the ΔM (B^*–B) measurement. The sum of uncertainties on the production rate arising from the fit and background shape is 5.4%.

7.3 Photon energy calibration

The energy scale of the reconstructed conversion photons has been checked by examining the value of the fitted invariant mass of π^0 peaks formed by pairs of converted photons. In the Monte Carlo the generated B^*–B mass difference is reconstructed accurately without bias, and so limits can be put on the accuracy of conversion reconstruction by determining the precision with which the Monte Carlo duplicates the π^0 mass found in the data. Combinations are made of pairs of reconstructed conversions where one of those conversions has an energy consistent with the spectrum from $B^* \to B\gamma$ (*i.e.* 100 MeV $< E_\gamma <$ 800 MeV) and fits are made to these distributions to reconstruct the π^0 invariant mass.

The fits are made using a quadratic polynomial to describe the background and an asymmetric Gaussian (see Section 7.1) for the π^0 mass peak. The asymmetric function is necessary to account for the effect of radiative losses from the e^+ and e^- tracks of the conversions that produce a tail on the low energy side of the π^0 mass peak. These fits are shown for data and Monte Carlo in Figure 6. The difference between Monte Carlo and data in the description of the radiative energy losses can also be seen in the B^* signal distributions (see Section 7.1).

The fitted values of the peak positions found in Monte Carlo and data are compared. In the data a fitted π^0 mass of 134.0 $\pm$ 1.5 MeV/c^2 is found, whilst in the Monte Carlo the same fit yields a value of 134.9 $\pm$ 0.8 MeV/c^2. These are consistent within errors and so the sum in quadrature of the uncertainties on these fits is taken to represent the knowledge of the accuracy of the converted photon energy scale. This is 1.7 MeV/c^2, corresponding to 1.3% of the π^0 mass.

This uncertainty has been applied to the final B^* sample by scaling the photon energy by $\pm$1.3%, resulting in the same relative change in the measured mass difference of $\pm$0.6 MeV/c^2.

7.4 Photon efficiency

Studies of the relative yield of photons in data and Monte Carlo indicate that the conversion rate in the data is duplicated in the Monte Carlo to within 2.8%, the Monte Carlo being in deficit. Photons in hadronic events are dominated by those coming from π^0 decays. The total π^0 rate in Z^0 decays has been measured [16] to a precision of 4.8%, and seen to agree well with the JETSET predictions. The precision of these measurements is taken as a measure of the uncertainty in the photon production rate in the Monte Carlo.

The photon efficiency is a strong function of the photon energy, and so the spin alignment of the B^* is considered as a source of uncertainty on this efficiency. The average of the B^* spin alignment measurements made at LEP [1] and that measurement made in Section 8

is consistent with no spin alignment: $\sigma_l/(\sigma_l + \sigma_t) = 0.33 \pm 0.04$. The Monte Carlo used to calculate the photon acceptance generates B^* mesons with no spin alignment. Recalculating the photon efficiency in the Monte Carlo with the spin alignment constrained to lie within this range results in an additional uncertainty of $\pm$ 5.0%. Summing the uncertainties arising from differences in the data and Monte Carlo conversion yield, the knowledge of the photon production rate and the spin alignment uncertainty gives a total uncertainty in the photon efficiency of $\pm$7.5%.

7.5 b purity

Systematic errors on the purity of the b hadron sample arise from uncertainties in the Monte Carlo including potential inaccuracies in the fragmentation functions used in the Monte Carlo prescription.

The size of any systematic uncertainty arising from the mismodelling of the b purity in the Monte Carlo is derived from the stability of the relative B^* production rate as a function of the b purity. The analysis has been repeated varying the cut on the artificial neural network output variable that largely determines the b purity. This results in an error of 3.0% being assigned to the production rate measurement, equivalent to an error of approximately 30% on the total non-b background fraction. The b purity has also been calculated from the data using a double tagging method and this is seen to be in good agreement with the purity estimated using the Monte Carlo.

There is a possibility that radiative decays of excited heavy baryons could contribute to the observed spectrum of photons in an inclusively reconstructed sample of b hadrons. However recent estimates suggest that the mass splitting between such states and non-excited b baryons is much smaller than the observed B^*–B splitting and that the production rate for such states is very small [17].

7.6 Mean B momentum

The accuracy of the b hadron momentum reconstruction has been investigated by repeating the analysis on the Monte Carlo using the generated photon four-vector and the reconstructed B meson to form Bγ combinations. This reproduces the generated B^*–B mass difference with no bias. However it is found that there is a systematic shift in the mean reconstructed B momentum, relative to the generated value, of approximately +500 MeV/c.

It is assumed that this effect may arise from the limitations of the b hadron reconstruction algorithm in correctly assigning tracks to vertices in the event, *i.e.* tracks may be systematically misassigned either to the b hadron or as fragmentation products. To investigate this phenomenon the Monte Carlo has been used to duplicate the effect of such 'track swapping', on the assumption that the 500 MeV/c shift can be modelled as the misassignment of one track with approximately this momentum. In each jet used in the analysis a search is made for a track with a momentum of this order that is clearly assigned to the b hadron, *i.e.* with a weight $\omega > 0.6$. The weight of that track is then set to zero, (*i.e.* it is unambiguously

assigned as a fragmentation track). A similar exercise has been performed to move fragmentation tracks into the b hadron. In addition to duplicating a possible cause of the observed momentum bias, this technique also serves as a test of the sensitivity of the reconstruction algorithm to such misassignments. A total error on the mass difference of ± 0.5 MeV/c^2 is assigned.

The systematic errors on the mass difference and production rate measurements are summarised in Table 1.

	$\Delta(\Delta M)$, MeV/c^2	$\Delta(\sigma_{\mathrm{B}^*}/\sigma_{\mathrm{B}})$,%
f_{B}	-	4.7
Monte Carlo	0.1	1.6
fit & normalisation	0.3	5.4
photon E calibration	0.6	-
photon efficiency	-	7.5
b purity	-	3.0
mean p_{B}	0.5	-
total	0.8	10.9

Table 1: Contributions to the systematic uncertainty on the measurement of the B^*–B mass difference and the B^* relative production rate measurement.

8 B^* helicity analysis

Since the $\mathrm{B}^* \to \mathrm{B}\gamma$ decay is electromagnetic, parity is conserved in this process. Thus, whilst the polarization of B^* mesons cannot be deduced from angular distributions, information on the B^* spin alignment can. B^* mesons are vector particles and so can be described by the polarization states ± 1 and 0 along their flight direction. The decays of the transverse polarization states, ± 1, follow an angular distribution given by $\frac{1}{2}(1 + \cos^2\theta^*)$, where θ^* is the angle between the produced photon and the B^* flight direction, in the B^* rest frame. The decays of the longitudinal polarization state, 0, follow an angular distribution given by $\sin^2\theta^*$. Spin counting suggests that the cross-section for the transverse states, σ_t, should be twice that of the longitudinal state, σ_l, and the $\cos\theta^*$ distribution should be flat. In such a picture $\sigma_l/(\sigma_l + \sigma_t) = 1/3$.

This behaviour has been investigated by examining the differential cross-section of the photon boosted into the B^* frame. Measurements of the helicity structure of the B^* meson have been extracted by fitting the relative contribution of the transverse and longitudinal states to the angular distribution of the photon in this frame.

The observed B^* meson sample is divided into 10 bins of $\cos\theta^*$, and the production rate analysis performed independently for each of these bins. The background estimation and fitting procedure is as performed on the entire data sample. Bin-by-bin acceptance corrections

are applied using measurements of photon efficiency extracted from Monte Carlo. The acceptance corrected result is shown in Figure 7. Only those errors uncorrelated bin-to-bin are shown on this figure and included in the fit to the data, since correlated errors do not affect the result of the spin alignment measurement. The photon efficiency is a sufficiently strong function of E_γ (see Section 5) that no meaningful measurement can be made for $\cos\theta^*$ below –0.4, where the laboratory frame photon energy is low.

The systematic errors on this plot are dominated by those terms arising from uncertainties in the photon acceptance as a function of the estimated helicity angle, θ^*. The systematic errors from both the photon acceptance correction and the uncertainty in the background subtraction are estimated by comparing the Monte Carlo and data $\cos\theta^*$ distributions. The sideband region 0.1 GeV/c^2 $< \Delta M <$ 0.2 GeV/c^2 contains almost no contribution from the B^* and so is used to quantify discrepancies in the shape of the two distributions, as shown in Figure 8. In this figure θ^* refers to the apparent photon-B^* angle in the B^* frame were these to be signal events. A systematic difference in the number of decays selected in data and Monte Carlo as a function of $\cos\theta^*$ is seen. The largest discrepancy between bins is $\pm 5\%$, and this is taken as the uncertainty on each bin in $\cos\theta^*$. There are significant contributions to the errors arising from the limited statistics of the Monte Carlo used in the bin-by-bin acceptance calculation, and in the background estimation.

This photon differential cross-section distribution has been fitted to the sum of the transverse and longitudinally polarized helicity states to yield their relative contribution. The relative fraction of the longitudinally polarized B^* state is measured to be

$$\sigma_l/(\sigma_l + \sigma_t) = 0.36 \pm 0.06(stat.) \pm 0.07(syst.)$$

and is entirely consistent with a simple spin counting picture. An analysis of this result in terms of the spin density matrix of the B^* meson is presented in [18].

9 Summary and conclusions

The OPAL data taken during running between 1991 and 1995 in the vicinity of the Z^0 have been analysed to observe the B^* meson via the process $B^* \to B\gamma$. The B meson has been reconstructed inclusively and the photon reconstructed where it has converted into an e^+e^- pair. The 4.1 million hadronic events of the data sample yielded 1894 ± 89 B^* candidates.

The B^*–B mass difference and the relative production rate of the B^* meson have been measured to be

$$\Delta M(B^* - B) = 46.2 \pm 0.3(stat.) \pm 0.8(syst.)\ \text{MeV}/c^2$$

and

$$\sigma_{B^*}/\sigma_B = 0.760 \pm 0.036(stat.) \pm 0.083(syst.),$$

respectively, where these measurements average over all B meson states formed with u, d and s quarks. These are seen to be consistent with current world averages of $\Delta M(B^* - B) = 45.7 \pm 0.4$ MeV/c^2, and $\sigma^*_B/\sigma_B = 0.75 \pm 0.04$, [15].

Additionally, the relative contribution of the longitudinally polarized B^* state has been measured, using the angular distribution of the photons in the B^* rest frame, to be

$$\sigma_l/(\sigma_l + \sigma_t) = 0.36 \pm 0.06(stat.) \pm 0.07(syst.),$$

consistent with the value expected from a spin counting picture.

Acknowledgements

We particularly wish to thank the SL Division for the efficient operation of the LEP accelerator and for their continuing close cooperation with our experimental group. In addition to the support staff at our own institutions we are pleased to acknowledge the
Department of Energy, USA,
National Science Foundation, USA,
Particle Physics and Astronomy Research Council, UK,
Natural Sciences and Engineering Research Council, Canada,
Israel Science Foundation, administered by the Israel Academy of Science and Humanities,
Minerva Gesellschaft,
Japanese Ministry of Education, Science and Culture (the Monbusho) and a grant under the Monbusho International Science Research Program,
German Israeli Bi-national Science Foundation (GIF),
Direction des Sciences de la Matière du Commissariat à l'Energie Atomique, France,
Bundesministerium für Bildung, Wissenschaft, Forschung und Technologie, Germany,
National Research Council of Canada,
Hungarian Foundation for Scientific Research, OTKA T-016660, and OTKA F-015089.

References

[1] ALEPH Collaboration, D. Buskulic *et al.*, Z. Phys. **C69** (1996) 393;
DELPHI Collaboration, P. Abreu *et al.*, Z. Phys. **C68** (1995) 353;
L3 Collaboration, M. Acciarri *et al.*, Phys. Lett. **B345** (1995) 589;
CLEO Collaboration, D.S. Akerib *et al.*, Phys. Rev. Lett. **67** (1991) 1692;
CUSB Collaboration, Q.W. Wu *et al.*, Phys. Lett. **B273** (1991) 177.

[2] 'QCD Event Generators', I.G. Knowles and T. Sjöstrand *et al.*, 'Physics at LEP2', G. Altarelli, T. Sjöstrand and F. Zwirner (editors), CERN Yellow Report 96-01.

[3] OPAL Collaboration, K. Ahmet *et al.*, Nucl. Inst. and Meth. **A305** (1991) 275.

[4] P.P. Allport *et al.*, Nucl. Inst. and Meth. **A324** (1993) 34;
P.P. Allport *et al.*, Nucl. Inst. and Meth. **A346** (1994) 476.

[5] OPAL Collaboration, G. Alexander *et al.*, Z. Phys. **C52** (1991) 175.

[6] OPAL Collaboration, R. Akers *et al.*, Z. Phys. **C63** (1994) 197.
The maximum half-angle of the cone was set to 0.65 radians.

[7] T. Sjöstrand, Comp. Phys. Comm. **39** (1986) 347;
M. Bengtsson and T. Sjöstrand, Comp. Phys. Comm. **43** (1987) 367;
M. Bengtsson and T. Sjöstrand, Nucl. Phys. **B289** (1987) 810;
T. Sjöstrand, CERN-TH/92-6488;
JETSET 7.4 is described in T. Sjöstrand, Comp. Phys. Comm. **82** (1994) 74.

[8] Parameter values were tuned to describe global event shape variables:
OPAL Collaboration, G. Alexander *et al.*, Z. Phys. **C69** (1996) 543.

[9] J. Allison *et al.*, Nucl. Inst. and Meth. **A317** (1992) 47.

[10] C. Peterson, D. Schlatter, I. Schmitt and P.M. Zerwas, Phys. Rev. **D27** (1983) 105.

[11] OPAL Collaboration, G. Alexander *et al.*, Z. Phys. **C66** (1995) 19.

[12] DELPHI Collaboration, P. Abreu *et al.*, Phys. Lett. **B345**, (1995) 598.

[13] E.J. Eichten, C.T. Hill and C. Quigg, Phys. Rev. Lett. **71** (1993) 4116.

[14] ALEPH Collaboration, D. Buskulic *et al.*, Phys. Lett. **B357**, (1995) 685;
OPAL Collaboration, R. Akers *et al.*, Z. Phys. **C69**, (1996) 195;
DELPHI Collaboration, P. Abreu *et al.*, Z. Phys. **C68**, (1996) 375.

[15] Particle Data Group, 'Review of Particle Physics', Phys. Rev. **D54**, (1996) 1.

[16] L3 Collaboration, M. Acciarri *et al.*, Phys. Lett. **B371**, (1996) 126;
DELPHI Collaboration, W. Adam *et al.*, Z. Phys. **C69**, (1996) 561;
ALEPH Collaboration, R. Barate *et al.*, 'Inclusive Production of Neutral Pions in Hadronic Z^0 Decays', CERN-PPE/96-168. (Submitted to Z. Phys.C.).

[17] E. Jenkins, 'Update of Heavy Baryon Mass Predictions', USCD/PTH 96-23.

[18] OPAL Collaboration, G. Alexander *et al.*, 'Study of $\phi(1020)$, $D^{*\pm}$ and B^* spin alignment in hadronic Z^0 decays', CERN-PPE/96-???.

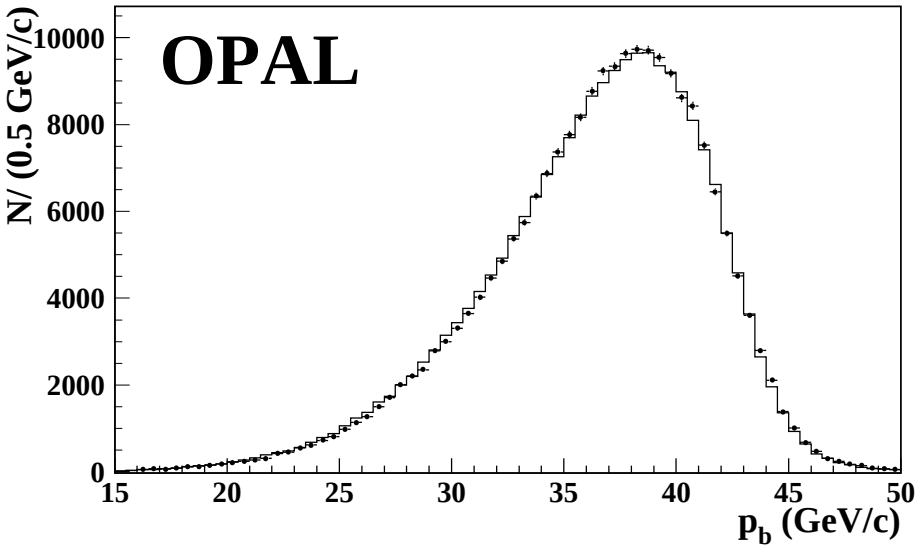

Figure 1: The reconstructed B hadron momentum distribution. The data are represented by points and the histogram represents the Monte Carlo simulation.

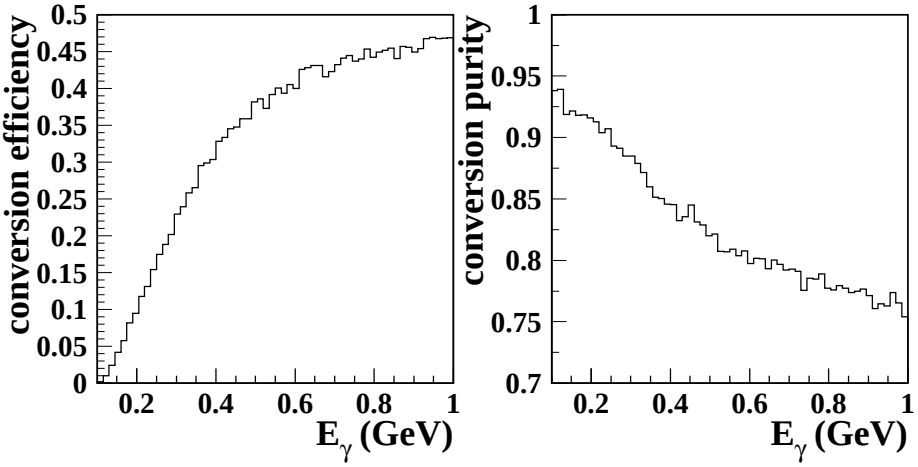

Figure 2: The efficiency and purity of the converted photon sample, as a function of the energy of the photon, as estimated by Monte Carlo simulation.

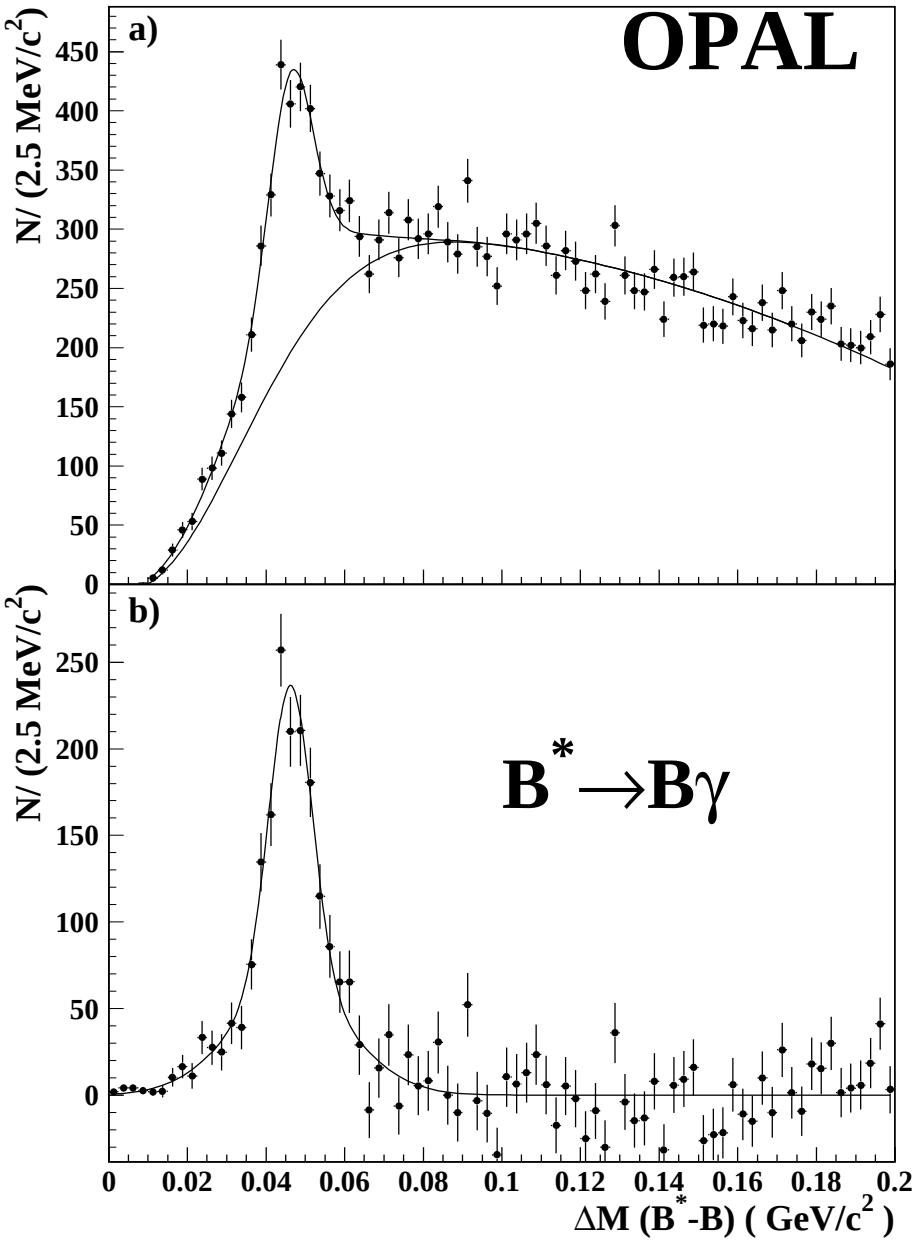

Figure 3: The B*–B mass difference distribution in data with *a)* a fit to the B* signal plus the Monte Carlo background estimate, and *b)* the fit to the B* signal with that background subtracted.

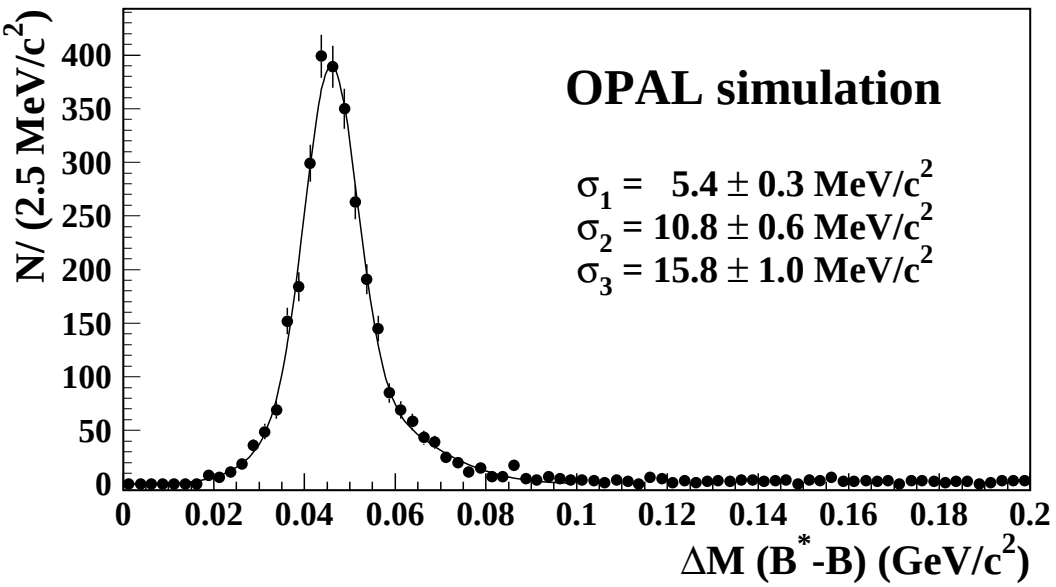

Figure 4: The B*–B mass difference distribution reconstructed in the Monte Carlo for *true* B*→B decays. The values of the fitted resolutions are shown: σ_1 is the width of the Gaussian, and σ_2 and σ_3 are the lower and upper widths of the asymmetric Gaussian, respectively.

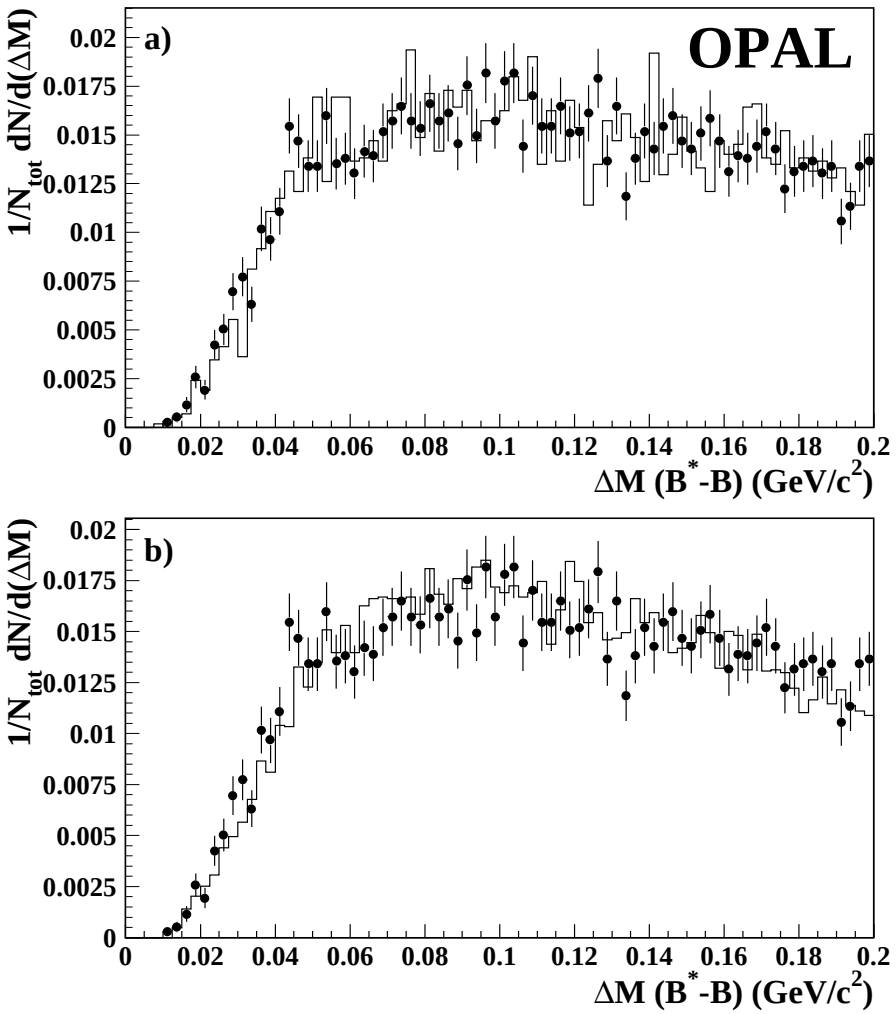

Figure 5: A comparison of the light quark, fake background (see text) from data (points) with a) the same distribution in Monte Carlo and, b) the Monte Carlo background used in the fit to the B^* signal.

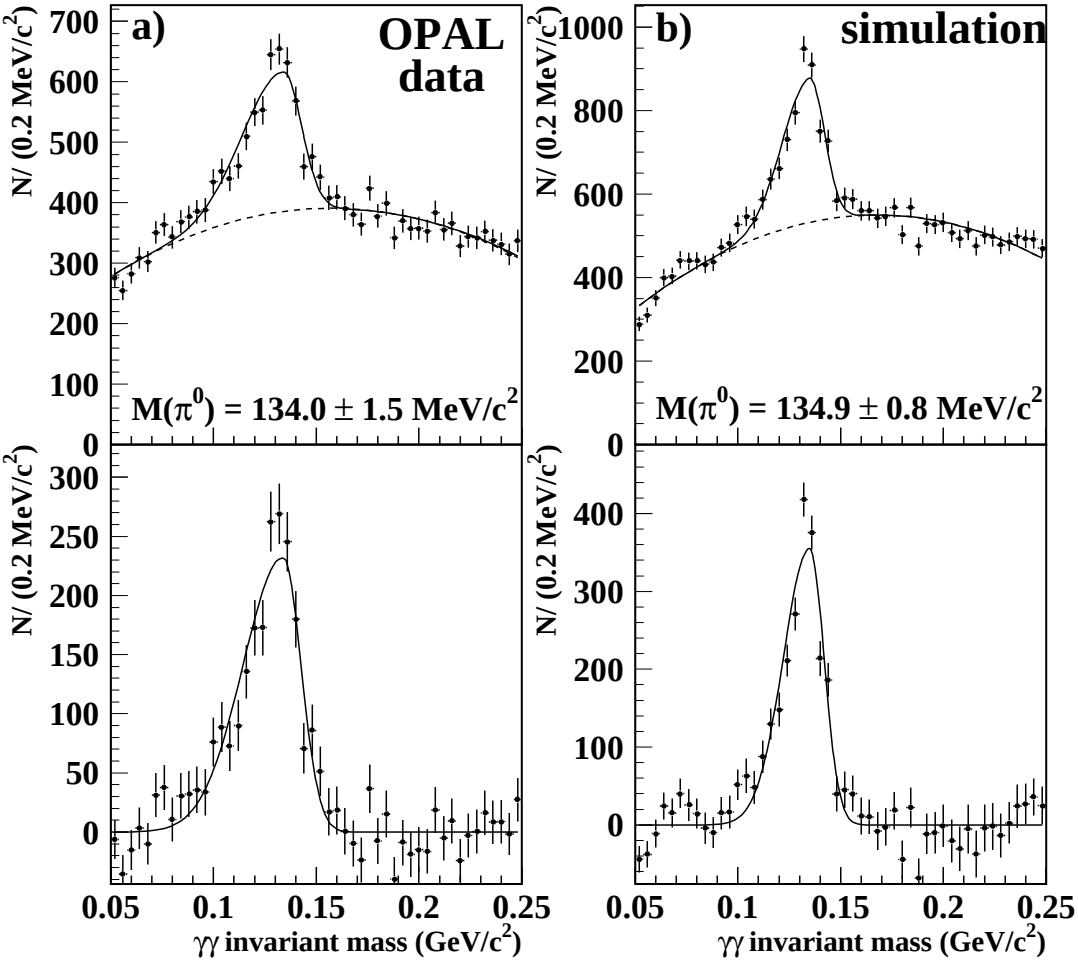

Figure 6: Fits to invariant mass distributions near the π^0 mass obtained by combining pairs of reconstructed conversions, for a) data and b) Monte Carlo. In each case the top plot shows a fit to the π^0 signal plus background and the lower plot shows the background subtracted signal. The discrepancy between the widths of the lower mass side of the distributions mirrors that seen between the B* signal in data and Monte Carlo.

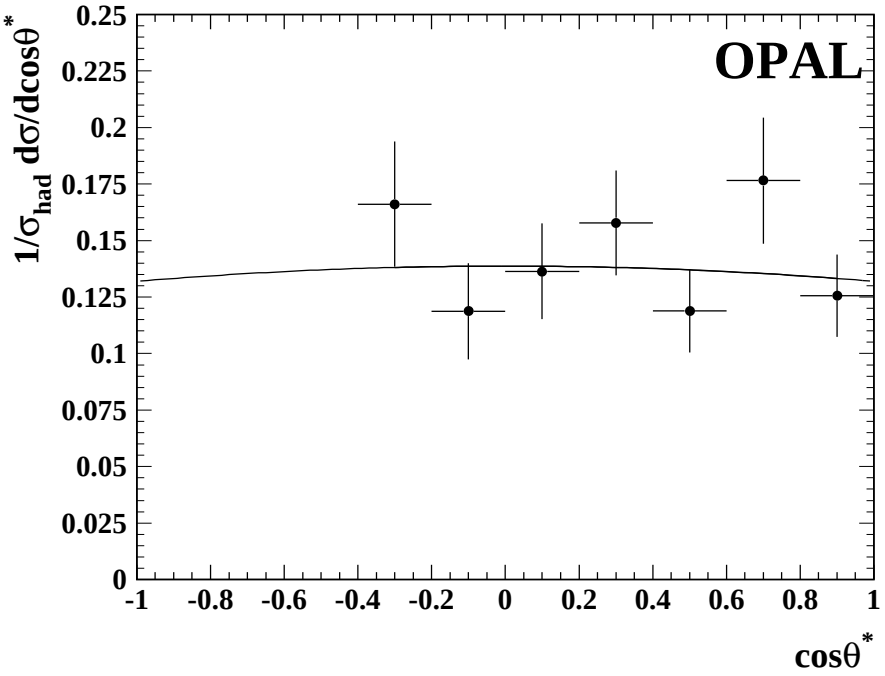

Figure 7: The acceptance and efficiency corrected angular distribution of the photon from the B^* decay in the rest frame of the B^*. (Only those errors uncorrelated bin-to-bin are shown.) The line shows the angular distribution that is expected from the relative contribution of transverse and longitudinal polarization states as determined from the fit to the data.

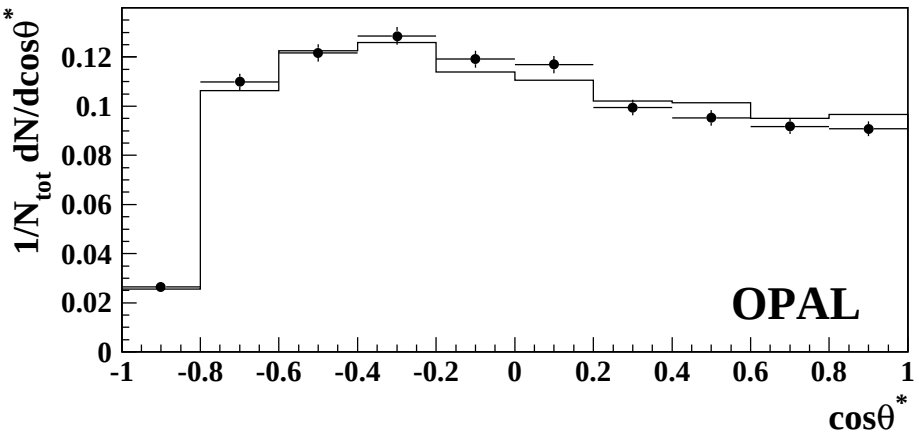

Figure 8: The measured $\cos\theta^*$ distribution of decays in the sideband region ($0.1\ \mathrm{GeV}/c^2 < \Delta M(\mathrm{B}^* - \mathrm{B}) < 0.2\ \mathrm{GeV}/c^2$) for data (points) and Monte Carlo (histogram).